THE JOURNAL OF BIOLOGICAL CHEMISTRY VOL. 286, NO. 39, pp. 34325–34334, September 30, 2011

A Structural Model of the Sgt2 Protein and Its Interactions with Chaperones and the Get4/Get5 Complex*[S]

Received for publication, June 30, 2011, and in revised form, July 18, 2011 Published, JBC Papers in Press, August 10, 2011, DOI 10.1074/jbc.M111.277798

Justin W. Chartron, Grecia M. Gonzalez, and William M. Clemons, Jr.[1]

From the Division of Chemistry and Chemical Engineering, California Institute of Technology, Pasadena, California 91125

The insertion of tail-anchored transmembrane (TA) proteins into the appropriate membrane is a post-translational event that requires stabilization of the transmembrane domain and targeting to the proper destination. Sgt2 is a heat-shock protein cognate (HSC) co-chaperone that preferentially binds endoplasmic reticulum-destined TA proteins and directs them to the GET pathway via Get4 and Get5. Here, we present the crystal structure from a fungal Sgt2 homolog of the tetratrico-repeat (TPR) domain and part of the linker that connects to the C-terminal domain. The linker extends into the two-carboxylate clamp of the TPR domain from a symmetry-related molecule mimicking the binding to HSCs. Based on this structure, we provide biochemical evidence that the Sgt2 TPR domain has the ability to directly bind multiple HSC family members. The structure allows us to propose features involved in this lower specificity relative to other TPR containing co-chaperones. We further show that a dimer of Sgt2 binds a single Get5 and use small angle x-ray scattering to characterize the domain arrangement of Sgt2 in solution. These results allow us to present a structural model of the Sgt2-Get4/Get5-HSC complex.

The eukaryotic cell is a complex environment of multiple membrane-bound organelles, each with a unique set of resident integral membrane proteins. Biogenesis of these proteins requires mechanisms for targeting and insertion into the correct membrane. For the majority destined to the ER[2] membrane, this is accomplished via the signal recognition particle pathway (1). Major exceptions to this rule are tail-anchor transmembrane (TA) proteins that are defined topologically by a single transmembrane helix within 30 residues of the C terminus. Examples are found in all membranes exposed to the cytoplasm (2, 3). A dedicated targeting pathway for ER-destined TA proteins has been elucidated and is called the GET pathway (Guided Entry of TA proteins) in yeast (4). The central player is Get3, a cytosolic ATPase that sequesters the transmembrane segment of a newly synthesized TA protein for targeting. A multiprotein complex consisting of Get4/Get5 and Sgt2 loads the TA protein onto Get3 (5). Get4 is an α-helical repeat protein that forms an obligate dimer with the N-terminal domain of Get5 (6–8), which also contains a ubiquitin-like domain and a C-terminal dimerization domain (6).

Sgt2, the small glutamine-rich tetratrico-repeat (TPR) containing protein (SGT in mammals), is a 38-kDa protein highly conserved across eukaryotes (9). It consists of an N-terminal homo-dimerization domain, a TPR domain composed of three TPR repeats, and a C-terminal domain that is rich in glutamine and methionine (10–12). The Sgt2 dimer has a larger hydrodynamic radius than expected for a globular protein suggesting an extended conformation (11, 12). SGT interacts with a variety of proteins, notably heat-shock proteins and their cognates (referred to here in general as HSC) such as Hsc70 and Hsp90, which bind directly to the TPR domain (11–14). SGT binding to HSCs appears to modulate the chaperone ATPase activity and folding rates dependent on other HSC co-chaperones. Binding to Hsc70 decreases ATPase activity and protein folding rates, whereas a neuronal Hsc70 complex, including SGT and cysteine string protein, stimulates ATPase activity (13, 15, 16). SGT also binds a number of viral proteins, and, in one case, the interaction was mediated by the TPR domain (17–19). The C-terminal domain of SGT is capable of binding hydrophobic regions of protein, such as the N-terminal signal sequence of myostatin and *in vitro* translated type 1 glucose transporter (11, 20).

The initial links between Sgt2 and Get5 were from proteome-wide yeast two-hybrid and tandem-affinity purification assays (21, 22). Additional yeast two-hybrid and pulldown assays demonstrated that an N-terminal construct of Sgt2 was necessary and sufficient for binding to Get5, and consequently Get4, in an interaction also dependent upon the Ubl domain of Get5 (7, 14). A direct role for Sgt2 in the TA targeting pathway was shown by two independent genetic interaction analyses indicating a strong functional connection with other GET pathway members (23, 24). Both demonstrated TA protein mis-localization in Sgt2 deletion strains, and Battle *et al.* (23) proposed that Sgt2 acts functionally upstream of Get5 and the other GET members. Most recently, it has been shown using an *in vitro* translation system that Sgt2 can bind to ER-destined TA proteins directly through the C-terminal hydrophobic-binding domain. With the aid of Get4/Get5, the TA protein is then transferred to Get3 (5). TA proteins destined to the mitochon-

* This work was supported, in whole or in part, by National Institutes of Health Grant R01GM097572 (to W. M. C.).

The atomic coordinates and structure factors (code 3SZ7) have been deposited in the Protein Data Bank, Research Collaboratory for Structural Bioinformatics, Rutgers University, New Brunswick, NJ (http://www.rcsb.org/).

[S] The on-line version of this article (available at http://www.jbc.org) contains supplemental Figs. S1–S3 and Table S1.

[1] Supported by the Searle Scholar program and a Burroughs-Wellcome Fund Career Award for the Biological Sciences. To whom correspondence should be addressed: M/C 114-96, 1200 E. California Blvd., Pasadena, CA 91104. Tel.: 626-395-1796; E-mail: clemons@caltech.edu.

[2] The abbreviations used are: ER, endoplasmic reticulum; TA, tail-anchor; HSC, heat-shock protein cognate; TPR, tetratrico-peptide repeat; GET, guided entry of TA proteins; SEC, size-exclusion chromatography; MALLS, multi-angle laser light scattering; SSRL, Stanford Synchrotron Radiation Laboratory; SAXS, small-angle X-ray scattering; HOP, Hsp organizing protein; CHIP, C terminus of Hsc70 interacting protein; *Af*Sgt2, Sgt2 from the filamentous fungus *A. fumigatus*.

dria do not bind Sgt2 directly but are bound to TPR domain-associated chaperones.

TPR domains are defined by a variable number of two-helix, 34-residue motifs and frequently mediate protein-protein interaction (25). A subclass acts as co-chaperones of HSCs by regulating nucleotide hydrolysis cycles, physically linking multiple HSC families, and/or connecting protein-folding pathways with alternate pathways such as ubiquitination and degradation (26). Examples are found in protein phosphatase 5, Hsp organizing protein (HOP in human, Sti1 in yeast) and C terminus of Hsc70 interacting protein (CHIP) (27–29). This TPR subclass is composed of three repeats followed in sequence by a C-terminal capping helix and recognizes the C-terminal residues of the HSC, exemplified by IEEVD in Hsc70 and MEEVD in Hsp90. Five conserved residues from the TPR domain mediate this interaction forming a motif named the two-carboxylate clamp, based on the recognition of the terminal acidic residue and the main-chain carboxylate (27).

Here we report the crystal structure of the Sgt2 TPR domain from the filamentous fungus *Aspergillus fumigatus* (*Af*Sgt2). A crystallographic contact generates a serendipitous interaction that mimics the carboxyl sequence of many HSCs binding to a TPR co-chaperone. Based on a structural analysis, we demonstrate biochemically that the Sgt2 TPR domain in *Saccharomyces cerevisiae* (Sgt2) can directly bind to at least four different HSC families. We also test the potential stoichiometry between Sgt2 and Get5 and characterize the structure of Sgt2 in solution, allowing us to present a structural model for the higher order complex between chaperones, Sgt2 and Get4/Get5.

EXPERIMENTAL PROCEDURES

Cloning, Expression, and Purification—Get4/Get5 was prepared as previously described (6). Sgt2, Ssa1, Sse1, Hsc82, and Hsp104 were amplified from genomic DNA isolated from *S. cerevisiae* strain S288C (*Af*Sgt2 from *A. fumigatus* strain 118, ATCC) and ligated into pET33b-derived vectors that added N-terminal hexahistidine tags separated by a tobacco etch virus protease site. Truncations were prepared by using QuikChange mutagenesis (Stratagene). Except for the crystallography, all experiments used Sgt2 and its variants from the *S. cerevisiae* homolog.

Sgt2 variants were expressed in *Escherichia coli* BL21(DE3)Star (Invitrogen). Cells were lysed by sonication, and proteins were purified by nickel affinity chromatography (Qiagen). Proteins were digested with tobacco etch virus protease for 3 h at room temperature, and uncut protein and protease were removed by incubation with nickel-nitrilotriacetic acid-agarose beads. Proteins were further purified by size-exclusion chromatography (SEC) using Superdex 200 or Superdex 75 (GE Healthcare) and concentrated to 10–20 mg/ml in 20 mM Tris, 100 mM NaCl, 5 mM 2-mercaptoethanol, pH 8.0. The molecular weight of the *Af*Sgt2 truncation product was determined by LC/MS at the Protein/Peptide MicroAnalytical Laboratory at Caltech.

Ssa1, Sse1, Hsc82, and Hsp104 were expressed in Rosetta(DE3) (Novagen), lysed by sonication in 50 mM K-HEPES, 300 mM KCl, 20 mM imidazole, 5 mM 2-mercaptoethanol, and 0.1% Triton X-100, pH 8.0 and purified by nickel affinity chromatography. Proteins were dialyzed against a buffer containing 0.1 mM EDTA during cleavage by tobacco etch virus protease and further purified by anion-exchange chromatography (ResourceQ, GE Healthcare) and SEC. Proteins were concentrated to 10–20 mg/ml in 20 mM K-HEPES, 100 mM KCl, 5 mM 2-mercaptoethanol, pH 8.0.

Pulldown Assays—Binding reactions between Get4/Get5 and Sgt2 were performed in 50 μl of a 10% slurry of nickel-nitrilotriacetic acid-agarose in a binding buffer of 20 mM Tris, 100 mM NaCl, 40 mM imidazole, pH 8.0. Per reaction, 8 μM of each protein was mixed for 10 min at room temperature. The resin was washed three times with 100 μl of binding buffer and eluted with binding buffer supplemented with 20 mM EDTA. Reactions between Ssa1, Sse1, Hsc82, and Hsp104 with the Sgt2 TPR domain were performed in 50 μl of 20 mM K-HEPES, 100 mM KCl, 20 mM imidazole, 5 mM $MgCl_2$, 5 mM ADP, 5 mM 2-mercaptoethanol, pH 7.5. 50 μM His-TPR domain were incubated with 5 μM chaperone on ice for 2 h and then added to 5 μl of nickel-nitrilotriacetic acid-agarose. The resin was washed twice with 100 μl of binding buffer and eluted with binding buffer with 300 mM imidazole.

SEC with MALLS—Complexes between Sgt2 and Get4/Get5 were formed in 20 mM Tris, 100 mM NaCl, 5 mM 2-mercaptoethanol, pH 7.0, and resolved by SEC using Superdex 200 or Superdex 75. To generate saturated complexes, 3-fold stoichiometric excesses of the smaller protein were used. Complex peaks were confirmed by SDS-PAGE, concentrated to 10 mg/ml, and separated on a Shodex KW-804 column with multiangle laser light scattering (MALLS) data collected by a DAWN HELEOS and Optilab rEX detector. Data were processed with ASTRA (Wyatt).

Crystallization—Crystallization screening was performed using the sitting drop vapor-diffusion method with commercially available screens (Hampton Research, Qiagen, Molecular Dimensions Ltd.) set up by a Mosquito robot (TTP Labtech) then incubated at room temperature. A proteolytic product of *Af*Sgt2 crystallized after 1 week as rectangular prisms against a reservoir of 25% PEG 1500 and 0.1 M MES/malic acid/Tris buffer, pH 4.0 (PACT Premier condition 37), with dimensions of $\sim 50 \times 50 \times 25$ μm. They were soaked in reservoir solution with glycerol added to 10% for 15 min, surrounded with perfluoropolyether PFO-X175/08 (Hampton Research) and flash frozen in liquid nitrogen.

Data Collection, Structure Solution, and Refinement—X-ray diffraction data were collected on beam line 12-2 at the Stanford Synchrotron Radiation Laboratory (SSRL) using a Pilatus 6M pixel array detector at 100 K. A complete dataset was collected from a single crystal to 1.72-Å resolution. Data were integrated, scaled, and merged using MOSFLM (30) and SCALA (31). Phases were determined by molecular replacement using the crystal structure of human SGT (PDB ID 2VYI) as a search model by PHASER (32), and the model was rebuilt using RESOLVE (33). The model was refined using COOT (34) and PHENIX (35). Secondary structure-matching root mean square deviation values were obtained using COOT. Solvent-accessible surface area between copies was calculated using PISA (36). Structure figures were prepared using PyMOL (37).

Small Angle X-ray Scattering—Samples were concentrated to 25 mg/ml and filtered through 0.22-μm membranes. Overnight dialysis was performed against 50 mM Tris, 100 mM NaCl, 5 mM 2-mercaptoethanol, pH 8.0. Dilutions to 1, 2, 5, and 10 mg/ml were made using the dialysate, and concentrations were determined using an ND-1000 spectrophotometer (Nanodrop Technologies) and theoretical extinction coefficients derived from protein sequences.

Data were collected at SSRL beam line 4-2 using a Rayonix MX225-HE detector, 1.13-Å wavelength x-rays, and a detector distance of 2.5 m. For each concentration, 20 exposures of 1 s were collected covering a momentum transfer range of 0.0055–0.3709 $Å^{-1}$. Data were reduced, averaged, and buffer-subtracted using MARPARSE (38). Extrapolation to infinite dilution and merging were performed with PRIMUS (39). Guiner analysis was performed using AutoRG, and distance distribution functions were determined with GNOM (40). *Ab initio* reconstructions were performed using software available in the ATSAS package (41). Sgt2-N and Sgt2-N-TPR were reconstructed with imposed 2-fold symmetry as an additional constraint on the data. Sgt2-N/Get5-Ubl was reconstructed without imposed symmetry.

RESULTS

Crystal Structure of a Fungal Sgt2 TPR Domain—We expressed the TPR and C-terminal domains of the *A. fumigatus* homolog of Sgt2 (*Af*Sgt2), corresponding to residues 109–341, in *E. coli* and purified it using nickel-nitrilotriacetic acid affinity chromatography. There was an extensive range of proteolysis, and two major species could be resolved by SEC (supplemental Fig. S1). The smaller protein is a proteolytic product with a molecular mass of 17,547 Da, consistent with the predicted molecular mass of residues 109–267. This protein yielded orthorhombic crystals in space group *F*222 that diffracted to a maximum of 1.72-Å resolution. The crystal structure was solved by molecular replacement using the human SGT α-isoform TPR domain (SGTA) (42) as a search model. A single copy of the TPR domain (*Af*Sgt2-TPR) was located in the asymmetric unit (Fig. 1*A*). Electron density extending from the C-terminal helix of the TPR domain could be modeled as 21 residues of the linker connecting to the C-terminal domain. Overall, unambiguous electron density throughout the entire chain allowed residues 109–254 to be modeled and refined to an R_{factor} of 0.1675 and an R_{free} of 0.2082. Complete crystallographic statistics are shown in supplemental Table S1.

The *Af*Sgt2-TPR has 38% sequence identity and 60% similarity to the SGTA TPR domain and shares an architecture consisting of three TPR repeats comprised by helices α1–α6 with a "capping" helix, α7 (Fig. 1, *A* and *E*). Like other domains composed of three TPR repeats, these seven helices are arranged in a right-handed supercoil (25) resulting in a concave surface lined by α1, α3, α5, and α7. The Cα root mean square deviation between the TPR domains of the SGTA and *Af*Sgt2 is 1.2 Å. Relative to the truncated SGTA construct, α7 is extended by five residues, and the angle formed between α6 and α7 is increased by ~10° (Fig. 1*B*). Unlike the SGTA crystal structure, which lacks extensive intermolecular contacts, *Af*Sgt2-TPR forms a crystallographic dimer with a symmetry-related copy, burying 2108 $Å^2$ of solvent-accessible surface area (Fig. 1*A*, *inset*). This interface is mediated by the α7 helices, which pack head-to-tail against one another, and residues 240–254 of the linker to the C-terminal domain, which bind into the TPR groove of the opposite copy in an extended conformation. This includes a well ordered interaction between two acidic side chains (Glu-239 to Asp-194) outside the groove that is unlikely to occur *in vivo* and may be stabilized by the low pH of crystallization.

Fortuitously, the sequence of residues 240–247 in *Af*Sgt2, PPADDVDD, resembles the C-terminal residues of Hsp70 and Hsp90 homologs, exemplified respectively in yeast by PTVEEVD in Ssa1 and TEMEEVD in Hsc82. These sequences are recognized by a variety of TPR domains containing a two-carboxylate clamp that anchors the EEVD motif (27). Hsp70/Hsp90 Organizing Protein (HOP) contains three TPR domains designated TPR1, TPR2a, and TPR2b. TPR1 specifically binds Hsc70, whereas TPR2a binds Hsp90, and the crystal structures of these interactions have allowed an understanding of determinants of substrate specificity in TPR domains (27, 43). The main chain conformation of the C-terminal linker region of *Af*Sgt2 in our crystal structure is identical to that of the GPTIEEVD peptide bound to HOP TPR1 (Fig. 1*C*). The two-carboxylate clamp is composed of five highly conserved residues that make hydrogen bonds to the main chain of the EEVD motif. In *Af*Sgt2, Arg-187 (Arg-175; for clarity when referencing the structure *A. fumigatus* numbering will be used and *S. cerevisiae* sequence numbering will be provided in parenthesis) and Lys-183 (Arg-171) interact with the carbonyl of Asp-244 and Arg-187 (Arg-175) makes an additional contact to the carbonyl of Asp-243 (Fig. 1*D*). Asn-122 (Asn-110) extends from α3 to form a hydrogen bond with Asn-153 (Asn-141) from α5, and these two asparagines hydrogen bond with the amide and carbonyl of Asp-246. Lys-118 (Lys-106) hydrogen bonds with the carbonyl of Asp-247, the equivalent position of the terminal carboxyl of Hsp70/90. In addition to these five canonical residues, Tyr-181 (Tyr-169), conserved across eukaryotes, forms a hydrogen bond with the side chain of Asp-246 (Fig. 1, *D* and *E*).

The TPR Domain of Sgt2 Is a General HSC Binding Interface—Sgt2 is physically linked with several families of heat-shock proteins. Hsp70 homologs Ssa1 and Ssa2, Hsp110 homologs Sse1 and Sse2, the Hsp90 homolog Hsc82, and the Hsp100 homolog Hsp104 co-purify with Sgt2 from yeast lysate, and all of these interactions are abolished by mutation of residues in the two-carboxylate clamp (5, 24). TPR domain containing co-chaperones often have specificity for different HSCs; therefore, we asked if Sgt2 can either bind each of these chaperone families directly or if co-immunoprecipitation of certain families were mediated by sub-complexes between chaperones. For example, Sse1 can form a stable complex with Ssa1 (44). SGT and a homolog from *C. elegans* can bind directly to either Hsp70 or Hsp90 (11–13). Using a nickel affinity pulldown assay, purified Ssa1 and Hsc82 bind directly to a polyhistidine-tagged TPR domain of Sgt2 (Fig. 2*A*, *lanes 1–2* and *4–5*). A triple mutant of the Sgt2-specific Y169F and the two-carboxylate clamp residues R171A and R175A (designated "FAA" corresponding to *Af*Sgt2 numbering Y181/K183/R187 (Fig. 1, *D* and *E*)), reduced binding to background levels (Fig. 2*A*, *lanes 3* and *6*). Hsp104 has a

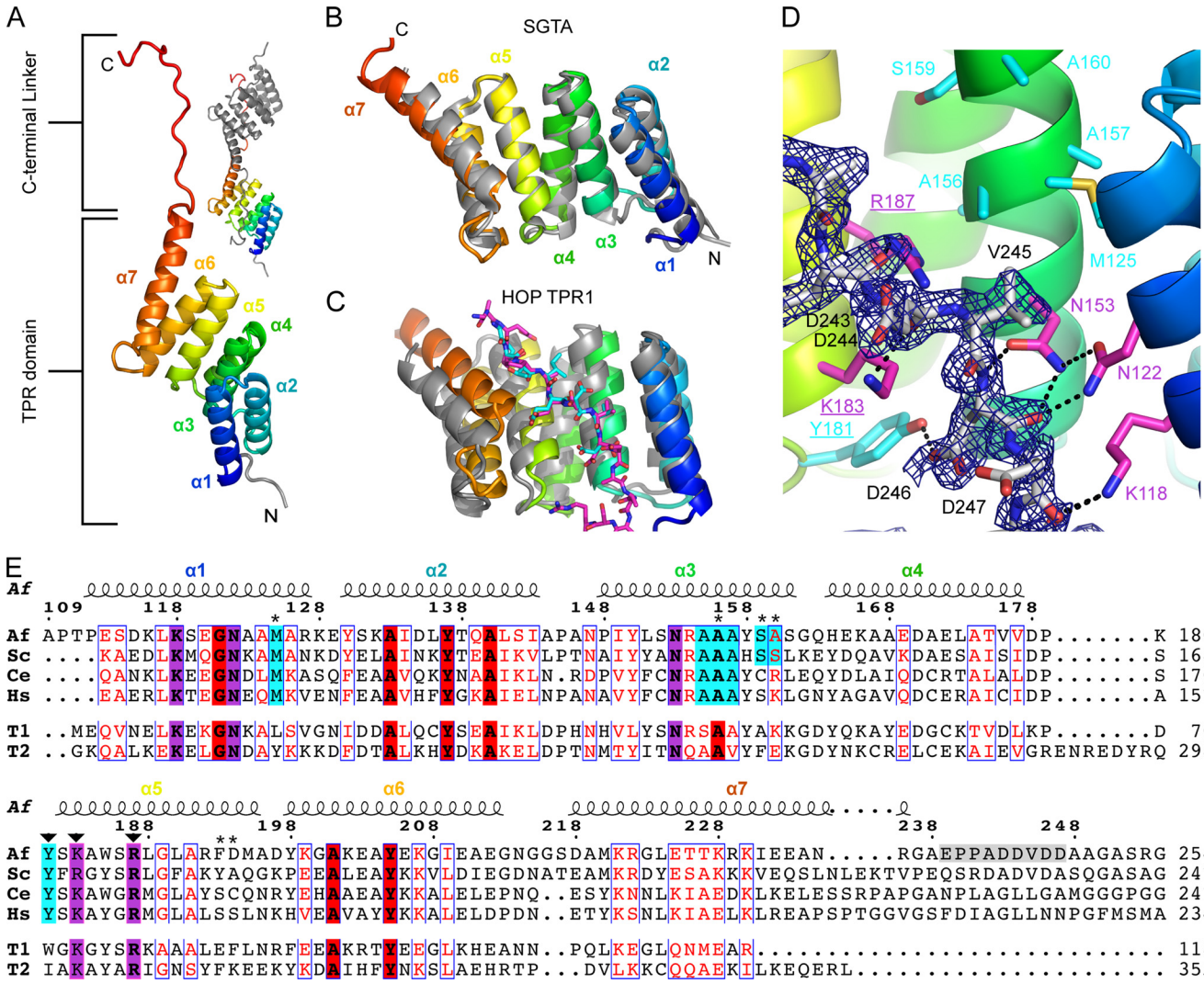

FIGURE 1. **Crystal structure of *Af*Sgt2 TPR domain.** *A*, the asymmetric unit shown as a *ribbons diagram* with *color* ramped from the N (*blue*) to C (*red*) termini. The region in *gray* is a cloning artifact. The crystallographic dimer is *inset*. *B*, *Af*Sgt2-TPR as in *A* superposed on human SGTA TPR domain (*gray*, PDBID 2VYI). *C*, superposition of *Af*Sgt2 and bound C-terminal linker (*rainbow*, *magenta carbons*) onto Hsc70 peptide-bound HOP TPR1A (*gray*, *cyan carbons*, PDBID 1ELW). *D*, *Af*Sgt2 TPR groove with a 1σ $2|F_o| - |F_c|$ simulated annealing omit map of the C-terminal linker of *Af*Sgt2 (*gray carbons*). Hydrogen bonds to conserved two-carboxylate clamp residues (*magenta carbons*) are indicated as *black dashes*. Residues are labeled based on the *Af*Sgt2 sequence. Sgt2-specific residues are shown as *cyan carbons*. The FAA mutant positions are *underlined*. *E*, alignment of the sequence observed in the crystal structure. Sequences are: *Af*, *A. fumigatus*; *Sc*, *S. cerevisiae*; *Ce*, *C. elegans*; *Hs*, *Homo sapiens*; *T1*, *H. sapiens* HOP TPR1; *T2*, *H. sapiens* HOP TPR2a. The *numbering above* is from *A. fumigatus*. Residues predicted to be involved in substrate specificity are marked with *asterisks*. The locations of the FAA mutations are indicated with *arrowheads*. Two-carboxylate clamp residues and conserved Sgt2 residues are highlighted in *magenta* and *cyan*, respectively. Further TPR conserved residues are highlighted in *red*. The C-terminal linker bound in the TPR groove is *highlighted* in *gray*.

C-terminal sequence of MEIDDDLD and binds to the two-carboxylate clamp in Cpr7 and the TPR1 domain of Sti1 (45). The C-terminal sequence of Sse1 is more divergent with the sequence EGDVDMD. Both Sse1 and Hsp104 bind to the TPR domain of Sgt2 dependent on the two-carboxylate clamp (Fig. 2*A*, *lanes 7–12*).

The structural basis for TPR domain specificity has been well characterized in HOP/Sti1. The TPR1 domain of HOP/Sti1 binds Hsp70 and Hsp100, whereas the TPR2A domain binds Hsp90 (27, 45). The identity of the hydrophobic residues preceding the EEVD terminus of Hsp70 and Hsp90 is critical for specific binding (46). Structure-guided mutational analysis determined a set of TPR residues that impact specificity, in particular TPR residues equivalent to positions Met-125 (Met-113), Ser-159 (Ser-147), and Ala-160 (Ser-148) in *Af*Sgt2 (Figs. 1*E* and 2*B*) (43). In HOP-TPR1, these positions are occupied by Leu-15, Ala-49, and Lys-50, and the isoleucine of the Hsp70 GPTIEEVD sequence fits between the alanine and lysine side chains on α3 (Fig. 2*C*). Alternatively, in HOP-TPR2a, the respective positions are occupied by Tyr-236, Phe-270, and Glu-271, and the methionine of the Hsp90 MEEVD sequence is found between α3 and α1 interacting with the tyrosine and glutamate (Fig. 2*D*). A structure of HOP-TPR2a bound with non-cognate Hsp70-derived peptide shows that the isoleucine is not accommodated and becomes solvent-exposed (47). In contrast with the HOP/Sti1 TPR domains, these positions in Sgt2 create an open pocket that we predict accommodates a wider range of substrates (Fig. 2*B*). Met-125 (Met-113) is conserved across the eukaryotic kingdom; Ser-159 (Ser-147) and Ala-160 (Ser-148) are highly conserved in fungi (Fig. 1*E*).

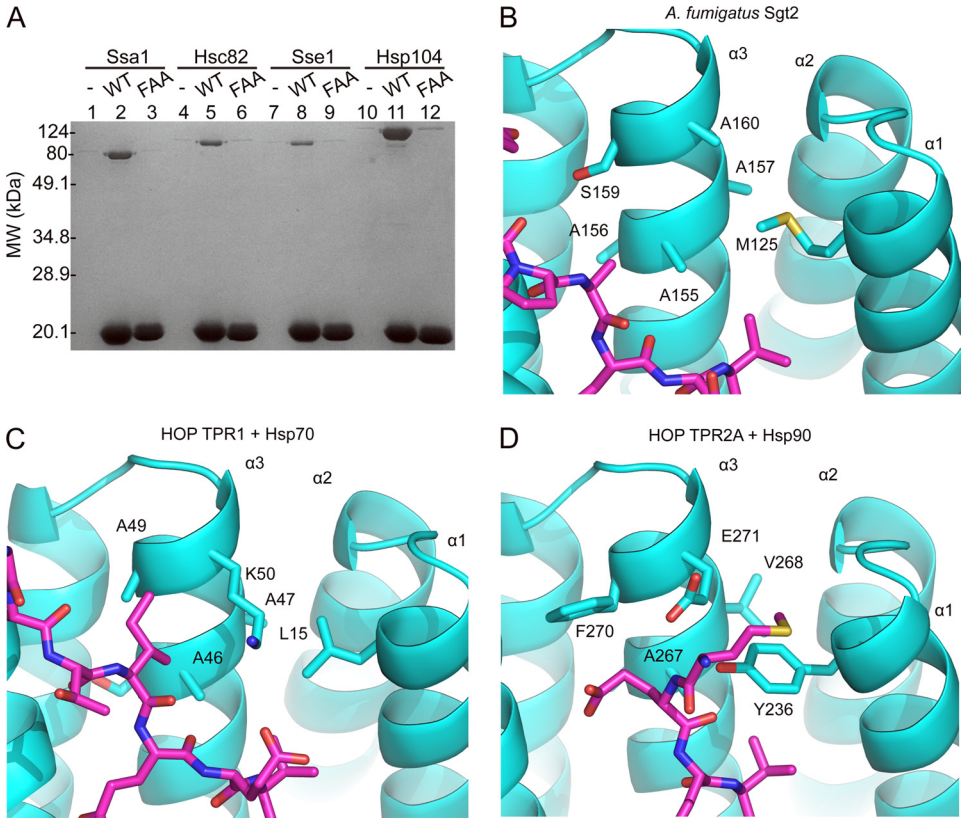

FIGURE 2. **Sgt2 binds multiple chaperone families.** *A*, SDS-PAGE of nickel affinity pulldown assays of Ssa1, Hsc82, Sse1, or Hsp104 in the absence of Sgt2 (−), with wild-type polyhistidine-tagged Sgt2-TPR (*WT*) or polyhistidine-tagged Sgt2-TPR-FAA (*FAA*). *B–D*, hydrophobic binding pocket on the TPR groove (*cyan*) with bound peptides (*magenta*) of *Af*Sgt2-TPR with symmetry molecule (*B*), *H. sapiens* HOP TPR1 with Hsp70-derived peptide (PDB ID 1ELW) (*C*), and *H. sapiens* HOP TPR2A with Hsp90-derived peptide (PDBID 1ELR) (*D*).

Higher eukaryotes have a conserved basic residue at position 160, perhaps indicating variation in specificity. Additionally, Ala-155 (Ala-143), Ala-156 (Ala-144), and Ala-157 (Ala-145) are strictly conserved in Sgt2 and complete the substrate interacting face of α3 (Figs. 1*E* and 2*B*).

Another characterized example of binding to multiple heat-shock protein families is the C-terminal TPR domain of Hsp70 interacting protein, CHIP, which can bind either Hsp70 or Hsp90. Structures with peptides derived from either chaperone show that, rather than binding in an extended conformation, the bound peptide kinks immediately prior to the EEVD motif to position the upstream isoleucine or methionine into a large hydrophobic pocket lined by α5, α6, and α7 that is unique to CHIP (29, 48).

The Sgt2 Dimer Binds a Single Copy of Get5 at a Canonical Ubl Interface—Yeast two-hybrid assays (7, 14) and analytical SEC (5) indicated that the N terminus of Sgt2 and the Ubl domain of Get5 are necessary for binding between these two proteins; however, molecular details of this interaction remain to be defined. We used a nickel affinity pulldown assay to further characterize the complex. Residue ranges of the domains of Sgt2 and Get5 are defined in Fig. 3*A*. Polyhistidine-tagged Get4/Get5 can bind Sgt2 (Fig. 3*B*, *lane 2*), as well as Get4/Get5ΔC (Fig. 3*B*, *lane 3*), indicating that dimerization of Get4/Get5 is not essential for the interaction. Further deletion of the Ubl domain abolishes binding to Sgt2 (Fig. 3*B*, *lane 4*). We previously identified a double mutant of Get5, L120A/K124A, that resulted in incomplete rescue of a Get5 deletion strain and is predicted to disrupt a conserved binding interface in ubiquitin-like domains (6, 49). Get4/Get5-L120A/K124A is unable to bind Sgt2 (Fig. 3*C*, *lane 5*). In the absence of Get4, recombinant Get5 is unstable and prone to forming inclusion bodies or susceptible to proteolysis (5, 6, 14). Removing the N-terminal Get4 binding domain results in a stable Get5-Ubl-C (6), which is capable of binding to Sgt2 (Fig. 3*C*, *lane 6*). We generated a construct of the N-terminal 72 residues of Sgt2. This minimal domain alone was sufficient to bind to Get4/Get5 (supplemental Fig. S2*A*). From this assay, we conclude that the interaction between Get4/Get5 and Sgt2 is predominantly between the Ubl domain of Get5, and the N-terminal domain of Sgt2 and is mediated by a canonical binding interface.

We next investigated the stoichiometry of the interaction between Sgt2 and Get5. After formation, complexes of Sgt2 and Get5 are stable and can be purified from unbound protein by SEC (supplemental Fig. S3). Purified complexes are stable upon further SEC and were subjected to SEC coupled with MALLS for molecular weight determination (Fig. 3*C* and Table 1). The Sgt2-N dimer possibly has two unique binding interfaces; therefore, up to two copies of Get5-Ubl might be expected to bind. However, only a single higher weight peak was observed after incubation with a 3-fold stoichiometric excess of Get5-Ubl (supplemental Fig. S3). The MALLS molecular weight of this complex was most consistent with an Sgt2-N dimer and a single copy of Get5-Ubl (Fig. 3*C*, *top*, and Table 1). Similarly,

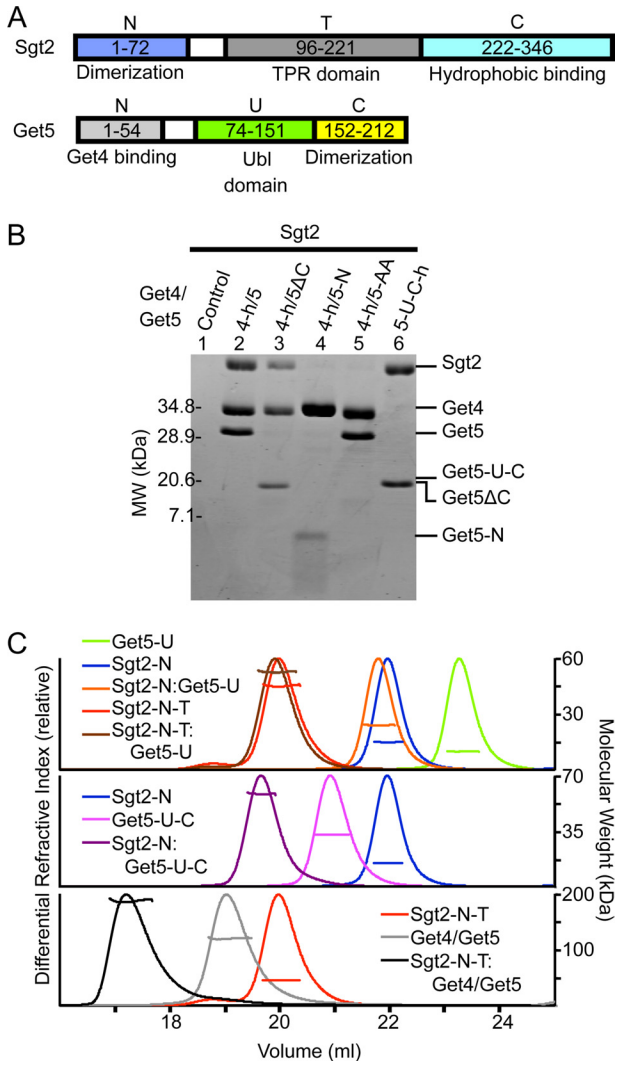

FIGURE 3. **The Sgt2-Get4/Get5 complex.** *A*, schematics indicating residue ranges of domains described in text with corresponding letter abbreviations. *B*, SDS-PAGE of nickel affinity pulldown assays. Get4 and Get5 are abbreviated as *4* and *5*, respectively, with "*h*" indicating the polyhistidine-tagged protein. *C*, SEC-MALLS of Sgt2 and Get4/Get5 complexes. *Traces* are normalized to maximum differential refractive index. *Horizontal lines* are experimentally measured molecular weight (*right axis*). Proteins added in 3-fold stoichiometric excess to generate complexes are Get5-Ubl (*top*), Sgt2-N (*middle*), Sgt2-N-TPR (*bottom*).

TABLE 1
SEC-MALLS- and SAXS-derived parameters

	Sequence molecular mass	MALLS molecular mass	SAXS	
			R_g	D_{max}
	kDa		*Å*	*Å*
Sgt2-N_{Dimer}	15.8	14.66	16.9	65
Sgt2-N-TPR_{Dimer}	49.1	44.8	42.5	155
Sgt2-TPR-$C_{Monomer}$			38.4[a]	122[a]
Get4/$Get5_{Dimer}$	120.0	119.4		
Get5-Ubl-C_{Dimer}	33.6	32.31		
Get5-$Ubl_{Monomer}$	10.0	9.68		
Complexes				
Get5-Ubl/Sgt2-N	25.7, 35.7[b]	23.78	20.7	70
Get5-Ubl/Sgt2-N-TPR	59.1, 69.1	52.19		
Sgt2-N/Get5-Ubl-C	49.4, 65.2	57.88		
Sgt2-N-TPR/Get4/Get5	169.1, 218.2	186.2		

[a] Values are the average for a 50-model ensemble selected by EOM (54).
[b] The molecular mass was estimated from sequences for 1:1 and 2:1 ratios.

when Sgt2-N-TPR was incubated with excess Get5-Ubl the determined molecular weight of the resulting complex was in closer agreement with a single bound copy of Get5-Ubl than two copies. Under the conditions tested here, we did not detect Sgt2 binding to more than one copy of Get5.

When Get5-Ubl-C was incubated with excess Sgt2-N, the resulting complex had a determined molecular mass of 57.88 kDa (Fig. 3*C*, *middle*). A complex of a Get5-Ubl-C dimer with a single Sgt2-N dimer has an expected molecular mass of 49.4 kDa and also with two Sgt2-N dimers of 65.2 kDa. When Get4/Get5 was incubated with excess Sgt2-N-TPR, the resulting complex had a molecular mass of 186 kDa, a value closer to a single copy of the Get4/Get5 dimer with a single copy of the Sgt2-N-TPR dimer (Fig. 3*C*, *bottom*). Although full-length Sgt2 can interact with Get4/Get5 (Fig. 3*B*), the same sample by SEC showed no higher peaks relative to each protein run individually. This could suggest a conformational change resulting in a similar hydrodynamic radius for the complex relative to the individual proteins; however, it is more likely that the complex simply was not stable by this method. It is possible that steric clashes between Get4 and the Sgt2-C domain, or increased entropic costs, reduce the binding affinity.

Ydj1 Does Not Directly Bind the Sgt2-Get4/Get5 Complex—The yeast DnaJ homolog Ydj1 is reported to bind Get5, which mediates a genetic interaction between Ydj1 and Sgt2 (14). In that study, recombinant Get5, in the absence of Get4, formed an *in vitro* complex with Ydj1. We tested whether Ydj1 binds to purified Get4/Get5 but did not see any enrichment in a pulldown assay, nor could we detect binding with the addition of Sgt2 or Ssa1 (supplemental Fig. S2*B*). The N-terminal domain of Get5 causes the protein to aggregate in the absence of Get4, and we propose that Ydj1 binds in response to this aggregation. Rather than directly interacting with Sgt2, Get4, or Get5, the genetic linkage is likely due to the role of Ydj1 in regulating Ssa1. It is noteworthy that Sis1, the other DnaJ homolog in yeast, co-immunoprecipitates with Sgt2 dependent upon two-carboxylate clamp (5).

SAXS of Sgt2—Sgt2 is a multidomain dimeric protein with an extended conformation whose domain arrangement is unknown. Small angle x-ray scattering (SAXS) allows determination of particle size, analysis of flexibility, and *ab initio* determination of low resolution structure. This allows modeling of higher order assemblies when coupled with high resolution structures of individual domains. SAXS was performed on Sgt2 using the constructs indicated in Table 1. Values for radius of gyration (R_g) and the maximum particle distance (D_{max}) were obtained from the indirect Fourier transform processed in GNOM. We generated *ab initio* models of Sgt2-N and Sgt2-N-TPR using GASBOR (50), which uses dummy residues restrained with simulated chain connectivity to fit experimental data. A total of 20 independent models was generated for each construct, and these were superposed, averaged, and filtered using DAMAVER (51). The resulting model represents the most probable volume shared by the individual models. Sgt2-N was reconstructed as a somewhat spherical particle, in agreement with the p(r) function, which has a single peak that smoothly approaches zero (Fig. 4, *A* and *B*). The p(r) function of Sgt2-N-TPR is indicative of multiple folded domains as it has

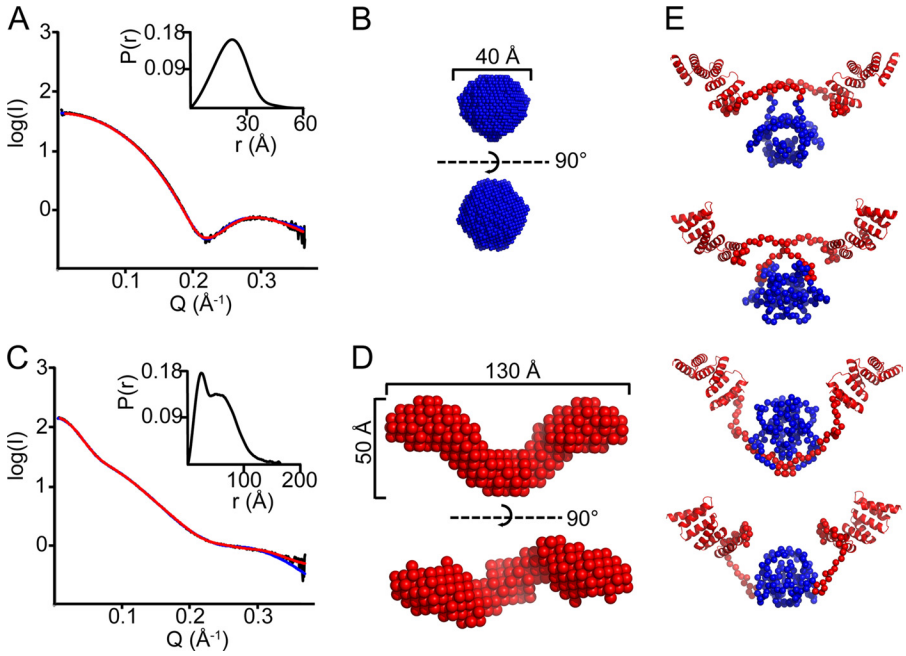

FIGURE 4. **SAXS of Sgt2-N and Sgt2-N-TPR.** *A* and *C*, experimental SAXS curve (*black*), fits of the best GASBOR (*red*) and BUNCH (*blue*) models and pair-probability functions (*inset*) for Sgt2-N (*A*) and Sgt2-N-TPR (*C*). *B* and *D*, *ab initio* reconstructions of 20 averaged and filtered GASBOR models of Sgt2-N (*B*) and Sgt2-N-TPR (*D*). *Bottom images* are rotated relative to *top images*. *E*, four example BUNCH models. *Blue regions* were fit to both Sgt2-N and Sgt2-N-TPR data, while *red regions* were fit to only Sgt2-N-TPR.

more than one peak (Fig. 4*C*). Sgt2-N-TPR reconstructed as a curved tubular shape, with two volumes, appropriately sized for TPR domains, extending out from the dimerization domain in the same plane (Fig. 4*D*). We additionally modeled Sgt2-N-TPR with the program BUNCH, which allows fitting to multiple SAXS curves in cases where scattering from truncations are available, and it also fits high resolution structures as rigid bodies (52). In this case, the fit utilized the TPR crystal structure and Sgt2-N curve in addition to the Sgt2-N-TPR curve. Unknown regions were generated *ab initio* as dummy residues. The resulting models are in agreement with the averaged GASBOR model (Fig. 4*E*). The orientation of the TPR domain groove is not resolved by SAXS; it may be resolution-limited or averaged due to flexibility in the inter-domain linker. Importantly, the angle formed between the TPR domains and the N-domain, as well as the end-to-end distance of the TPR domains is consistent between models from multiple methods.

From primary sequence, Sgt2-TPR-C is expected to have high flexibility, and the shape of the Kratky plot is characteristic of a partially folded protein as intensity plateaus to a non-zero value as *Q* increases (53) (Fig. 5*A*). The program EOM interprets SAXS data of flexible proteins by selecting ensembles of structures to fit scattering from a large, diverse pool of structures (54). The *Af*Sgt2-TPR crystal structure was linked with 10,000 random C_α models of the C-terminal domain. An ensemble of 50 structures was fit to the data (Fig. 5*B*). The R_g and D_{max} distributions (Fig. 5, *C* and *D*) of the fitted structures have similar center and shape to the entire random pool of structures, indicating unrestricted flexibility between the TPR and C-terminal domains.

We further used SAXS to confirm the stoichiometry between Sgt2 and Get5. Using data for the purified Sgt2-N/Get5-Ubl complex, the molecular envelope was reconstructed with the

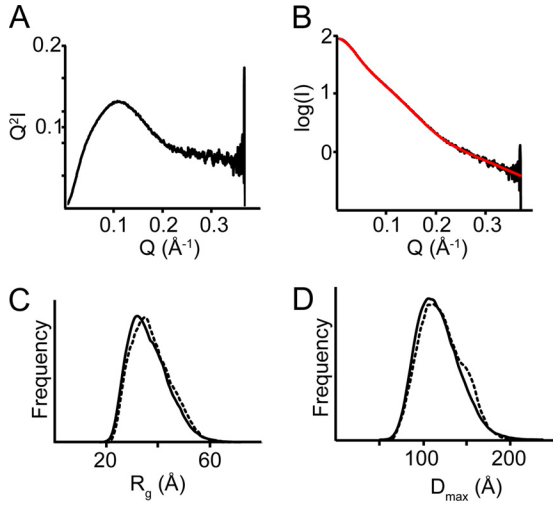

FIGURE 5. **SAXS of the flexible Sgt2-TPR-C.** *A*, Kratky plot; *B*, experimental SAXS curve of Sgt2-TPR-C (*black*) with EOM fit (*red*); *C* and *D*, R_g and D_{max} distributions, respectively, for 10,000 random C-domain models relative to the TPR domain (*dashed lines*) *versus* 50 models fit to experimental data (*solid lines*). Correlation suggests unrestricted motion of the C-domain relative to the TPR domain.

program DAMMIF (Fig. 6, *A* and *B*). DAMMIF uses dummy atoms to fill a volume that satisfies the SAXS curve and, unlike GASBOR, does not require total residue number as an input, reducing bias of the complex stoichiometry. The averaged model is ellipsoidal, with a long dimension of ~60 Å. This can only be fit with the 40-Å diameter reconstruction of the Sgt2-N dimer (Fig. 4*B*) and a single Get5-Ubl of ~20-Å diameter, previously modeled from an NMR structure (Fig. 6*C*) (6).

DISCUSSION

The mechanism for the sorting of TA proteins among the variety of target membranes is only beginning to be understood.

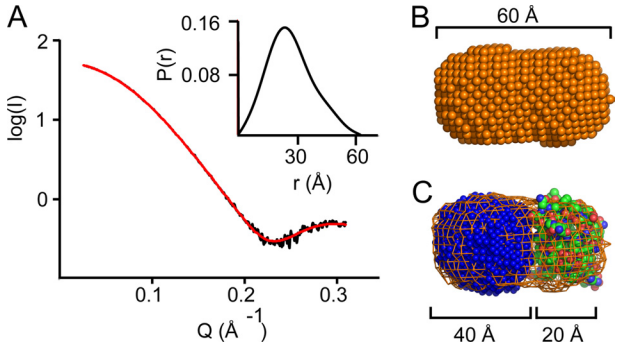

FIGURE 6. **SAXS of an Sgt2/Get5 complex.** *A*, experimental SAXS curve (*black*) *versus* fit of the best DAMMIF model (*red*). The pair-probability function of Sgt2-N/Get5-U is *inset*. *B*, filtered average of 20 DAMMIF models. *C*, filtered average GASBOR model of Sgt2-N (*blue spheres*) and space filling model of a homology model of Get5-Ubl (*green*) fit into the filtered average model of Sgt2-N/Get5-Ubl (*orange mesh*).

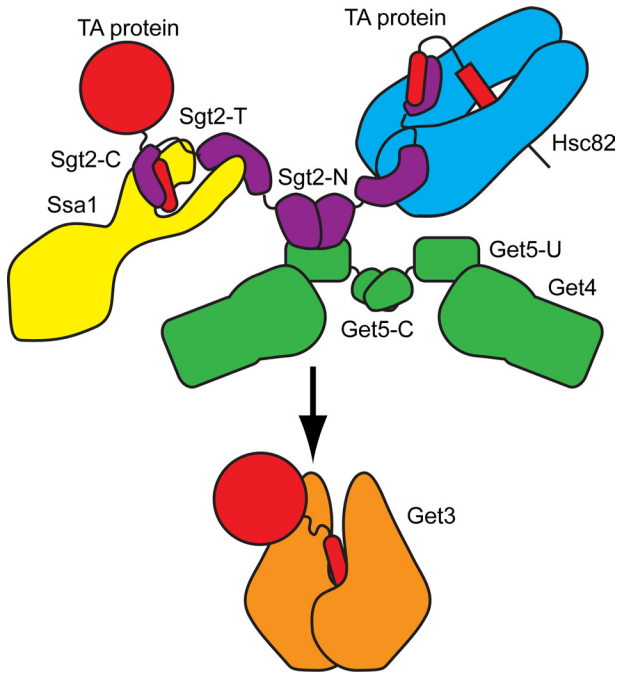

FIGURE 7. **Model for the Sgt2/Get4/Get5/HSC complex.** Sgt2 (*purple*) is bound to Get4/Get5 via the Ubl domain (*green*). TA protein (*red*) transmembrane domain may initially be in complex with an HSC (*e.g.* with Ssa1, *yellow*) with subsequent binding to the Sgt2-TPR and transfer to Sgt2-C. Alternatively, the transmembrane domain initially binds to Sgt2-C and chaperones required for substrate stabilization are bound to the Sgt2-TPR. The complex then releases the TA protein to Get3.

Sgt2 appears to selectively bind ER-destined TA proteins transferring these substrates with the aid of Get4/Get5 to Get3. Sgt2 contains a TPR domain that physically links the GET pathway to other chaperone pathways. Although other characterized TPR domain-containing co-chaperones are limited in their binding to one or two heat-shock protein families, we demonstrate here that the Sgt2 TPR domain can bind directly to members of at least four families. This promiscuity is explained by the structure of the Sgt2 TPR domain. A phylogenetic analysis of TPR domain sequences indicated that the Sgt2 TPR domain is most similar to the HOP domains (55) and, indeed, in our structure, bound peptide adopts an identical conformation. The determinants of substrate specificity include the conserved binding pocket formed by residues Met-125 (Met-113), Ala-155 (Ala-143), Ala-156 (Ala-144), Ala-157 (Ala-145), Ser-159 (Ser-147), and Ala-160 (Ser-148). This wider pocket is sterically less restrictive than the HOP TPR domains presumably allowing for the binding of non-canonical two-carboxylate clamp substrates such as the EGDVDMD of Sse1. Moreover, human SGTA TPR can interact with an internal stretch in the androgen receptor that does not contain a clear binding motif suggesting an even broader specificity (56). In addition to the five two-carboxylate clamp residues, a conserved tyrosine contributes a hydrogen bond to the side chain of the residue corresponding to the terminal residue in Hsp70 or Hsp90. It is possible that this further stabilizes binding to longer sequences.

Is it simply fortuitous that the linker following the *Af*Sgt2 TPR contains the sequence PPADDVDD, resembling an HSC termini? Evidence for a possible functional role is that the sequence is conserved in the Eurotiomycetes family, of which *A. fumigatus* is a member, and *S. cerevisiae* Sgt2 contains the related sequence SRDADVDA (Fig. 1*E*). Unfortunately, similar regions are not found more broadly in other fungal homologs, and there are no comparable sequences found in higher eukaryotes. This does not rule out family-specific specialization, perhaps binding other co-chaperones; however, it makes a general conserved role for this sequence unlikely.

Sgt2 forms a direct complex with Get4/Get5 mediated by the dimerization domain of Sgt2 and the Ubl domain of Get5. Despite possible symmetry of Sgt2-N, only a single copy of Get5-Ubl can bind with high affinity. The Vps9-CUE domain is a homo-dimeric α-helical domain that binds ubiquitin at its symmetry axis and undergoes a conformational change that breaks symmetry to resemble a ubiquitin-associating domain (57). The Sgt2/Get5 complex may undergo similar rearrangements. Alternatively, binding of one copy may simply occlude a second binding site. The inability of Sgt2 to bind a second Ubl domain creates a potential for the Get4/Get5 dimer to bind two dimers of Sgt2. *In vitro*, complexes between the minimal binding domains are stable indefinitely; however, as additional domains are included only a single dimer of Sgt2 can bind Get4/Get5, and the full-length proteins do not form a complex stable over SEC. This leaves the overall *in vivo* stoichiometry ambiguous. It is likely that other factors, such as the Get4 to Get3 interaction, may result in a dynamic complex.

Based on the data we present here we can suggest an updated model for the role of Sgt2 in TA targeting and an overall structure of the Sgt2/Get4/Get5/HSC complex (Fig. 7). The SAXS analysis of Sgt2-N-TPR suggests that the TPR domains have independent motion. Coupled with the observations that N-domain deletions still bind both HSC and TA proteins (5), we conclude that the two Sgt2-TPR-C domains act independently. This would allow for the Sgt2 dimer to bind multiple HSCs simultaneously. The dimerization domain of Sgt2 would bind one Ubl of the Get4/Get5 hetero-tetramer. Sgt2 will sequester an ER-bound TA and deliver it specifically to Get3.

This work allows us to speculate on the interplay of HSCs and the GET pathway. The low specificity for HSC families suggests that Sgt2 can interact with unfolded proteins distributed among the majority of protein folding pathways in the cell. This may allow Sgt2 to act as a general recovery pathway for TA

proteins through its TPR domain, consistent with a recent observation that the TPR domain is not essential for targeting of certain substrates by Get3 under low stress conditions (58). Perhaps more prominently, given the genetic role of Sgt2 in the GET pathway, Sgt2 uses the TPR domain to couple multiple folding pathways with TA targeting. This would allow TA substrates with a variety of folding needs to enter the GET pathway. Combined, this suggests two possible routes for TA proteins through Sgt2: either HSCs bind the TA protein first and deliver them to Sgt2, or Sgt2 binds the TA first and chaperones are recruited to either aid in folding or to act as acceptors if the TA protein is not ER-destined.

TA proteins are diverse with the majority specifically targeted to either the ER or mitochondria. For those destined to the ER, both the GET pathway and Hsp70 operate post-translational targeting pathways, the former being critical as TA hydrophobicity increases (59). Targeting of TA proteins to the mitochondria is less characterized. It has been suggested that this may only depend on Hsp70/90-mediated targeting to the co-chaperone TPR receptors on the mitochondria (60, 61). This type of targeting could be more general as co-chaperone TPR receptors exist on every organelle (55, 62). These overlapping or alternative pathways may allow delivery independent of the GET pathway, possibly explaining why none of the individual GET components are essential under optimal conditions. All of this would suggest an important role for co-chaperone TPR proteins in delivery of TA proteins. Sgt2 would be the central co-chaperone acting as a sortase to optimize correct delivery to the GET pathway. If so, TA targeting by Sgt2 may be more akin to panning for gold, retaining substrate proteins for entry to the GET pathway from different points in protein biogenesis.

Acknowledgments—We thank D. C. Rees and S. O. Shan for critical reading of the manuscript. We thank members of the laboratory for support and useful discussions. We thank Graeme Card, Ana Gonzalez, and Michael Soltice for help with data collection at SSRL BL12-2, Tsutomu Matsui and Hiro Tsuruta for help with data collection and processing at the bioSAXS SSRL BL4-2, and Troy Walton for help with MALLS. We are grateful to Gordon and Betty Moore for support of the Molecular Observatory at Caltech.

REFERENCES

1. Walter, P., and Johnson, A. E. (1994) *Annu. Rev. Cell Biol.* **10,** 87–119
2. Kutay, U., Hartmann, E., and Rapoport, T. A. (1993) *Trends Cell Biol.* **3,** 72–75
3. Borgese, N., Brambillasca, S., and Colombo, S. (2007) *Curr. Opin. Cell Biol.* **19,** 368–375
4. Schuldiner, M., Metz, J., Schmid, V., Denic, V., Rakwalska, M., Schmitt, H. D., Schwappach, B., and Weissman, J. S. (2008) *Cell* **134,** 634–645
5. Wang, F., Brown, E. C., Mak, G., Zhuang, J., and Denic, V. (2010) *Mol. Cell* **40,** 159–171
6. Chartron, J. W., Suloway, C. J., Zaslaver, M., and Clemons, W. M., Jr. (2010) *Proc. Natl. Acad. Sci. U.S.A.* **107,** 12127–12132
7. Chang, Y. W., Chuang, Y. C., Ho, Y. C., Cheng, M. Y., Sun, Y. J., Hsiao, C. D., and Wang, C. (2010) *J. Biol. Chem.* **285,** 9962–9970
8. Bozkurt, G., Wild, K., Amlacher, S., Hurt, E., Dobberstein, B., and Sinning, I. (2010) *FEBS Lett.* **584,** 1509–1514
9. Kordes, E., Savelyeva, L., Schwab, M., Rommelaere, J., Jauniaux, J. C., and Cziepluch, C. (1998) *Genomics* **52,** 90–94
10. Tobaben, S., Varoqueaux, F., Brose, N., Stahl, B., and Meyer, G. (2003) *J. Biol. Chem.* **278,** 38376–38383
11. Liou, S. T., and Wang, C. (2005) *Arch. Biochem. Biophys.* **435,** 253–263
12. Worrall, L. J., Wear, M. A., Page, A. P., and Walkinshaw, M. D. (2008) *Biochim. Biophys. Acta* **1784,** 496–503
13. Angeletti, P. C., Walker, D., and Panganiban, A. T. (2002) *Cell Stress Chaperones* **7,** 258–268
14. Liou, S. T., Cheng, M. Y., and Wang, C. (2007) *Cell Stress Chaperones* **12,** 59–70
15. Tobaben, S., Thakur, P., Fernández-Chacón, R., Südhof, T. C., Rettig, J., and Stahl, B. (2001) *Neuron* **31,** 987–999
16. Wu, S. J., Liu, F. H., Hu, S. M., and Wang, C. (2001) *Biochem. J.* **359,** 419–426
17. Callahan, M. A., Handley, M. A., Lee, Y. H., Talbot, K. J., Harper, J. W., and Panganiban, A. T. (1998) *J. Virol.* **72,** 5189–5197
18. Fielding, B. C., Gunalan, V., Tan, T. H., Chou, C. F., Shen, S., Khan, S., Lim, S. G., Hong, W., and Tan, Y. J. (2006) *Biochem. Biophys. Res. Commun.* **343,** 1201–1208
19. Cziepluch, C., Kordes, E., Poirey, R., Grewenig, A., Rommelaere, J., and Jauniaux, J. C. (1998) *J. Virol.* **72,** 4149–4156
20. Wang, H., Zhang, Q., and Zhu, D. (2003) *Biochem. Biophys. Res. Commun.* **311,** 877–883
21. Uetz, P., Giot, L., Cagney, G., Mansfield, T. A., Judson, R. S., Knight, J. R., Lockshon, D., Narayan, V., Srinivasan, M., Pochart, P., Qureshi-Emili, A., Li, Y., Godwin, B., Conover, D., Kalbfleisch, T., Vijayadamodar, G., Yang, M., Johnston, M., Fields, S., and Rothberg, J. M. (2000) *Nature* **403,** 623–627
22. Krogan, N. J., Cagney, G., Yu, H., Zhong, G., Guo, X., Ignatchenko, A., Li, J., Pu, S., Datta, N., Tikuisis, A. P., Punna, T., Peregrin-Alvarez, J. M., Shales, M., Zhang, X., Davey, M., Robinson, M. D., Paccanaro, A., Bray, J. E., Sheung, A., Beattie, B., Richards, D. P., Canadien, V., Lalev, A., Mena, F., Wong, P., Starostine, A., Canete, M. M., Vlasblom, J., Wu, S., Orsi, C., Collins, S. R., Chandran, S., Haw, R., Rilstone, J. J., Gandi, K., Thompson, N. J., Musso, G., St Onge, P., Ghanny, S., Lam, M. H., Butland, G., Altaf-Ul, A. M., Kanaya, S., Shilatifard, A., O'Shea, E., Weissman, J. S., Ingles, C. J., Hughes, T. R., Parkinson, J., Gerstein, M., Wodak, S. J., Emili, A., and Greenblatt, J. F. (2006) *Nature* **440,** 637–643
23. Battle, A., Jonikas, M. C., Walter, P., Weissman, J. S., and Koller, D. (2010) *Mol. Syst. Biol.* **6,** 379
24. Costanzo, M., Baryshnikova, A., Bellay, J., Kim, Y., Spear, E. D., Sevier, C. S., Ding, H., Koh, J. L., Toufighi, K., Mostafavi, S., Prinz, J., St Onge, R. P., VanderSluis, B., Makhnevych, T., Vizeacoumar, F. J., Alizadeh, S., Bahr, S., Brost, R. L., Chen, Y., Cokol, M., Deshpande, R., Li, Z., Lin, Z. Y., Liang, W., Marback, M., Paw, J., San Luis, B. J., Shuteriqi, E., Tong, A. H., van Dyk, N., Wallace, I. M., Whitney, J. A., Weirauch, M. T., Zhong, G., Zhu, H., Houry, W. A., Brudno, M., Ragibizadeh, S., Papp, B., Pál, C., Roth, F. P., Giaever, G., Nislow, C., Troyanskaya, O. G., Bussey, H., Bader, G. D., Gingras, A. C., Morris, Q. D., Kim, P. M., Kaiser, C. A., Myers, C. L., Andrews, B. J., and Boone, C. (2010) *Science* **327,** 425–431
25. D'Andrea, L. D., and Regan, L. (2003) *Trends Biochem. Sci.* **28,** 655–662
26. Meacham, G. C., Patterson, C., Zhang, W., Younger, J. M., and Cyr, D. M. (2001) *Nat. Cell Biol.* **3,** 100–105
27. Scheufler, C., Brinker, A., Bourenkov, G., Pegoraro, S., Moroder, L., Bartunik, H., Hartl, F. U., and Moarefi, I. (2000) *Cell* **101,** 199–210
28. Das, A. K., Cohen, P. W., and Barford, D. (1998) *EMBO J.* **17,** 1192–1199
29. Zhang, M., Windheim, M., Roe, S. M., Peggie, M., Cohen, P., Prodromou, C., and Pearl, L. H. (2005) *Mol. Cell* **20,** 525–538
30. Battye, T. G., Kontogiannis, L., Johnson, O., Powell, H. R., and Leslie, A. G. (2011) *Acta Crystallogr. D Biol. Crystallogr.* **67,** 271–281
31. Evans, P. (2006) *Acta Crystallogr. D Biol. Crystallogr.* **62,** 72–82
32. McCoy, A. J., Grosse-Kunstleve, R. W., Adams, P. D., Winn, M. D., Storoni, L. C., and Read, R. J. (2007) *J. Appl. Crystallogr.* **40,** 658–674
33. Terwilliger, T. C. (2003) *Acta Crystallogr. D Biol. Crystallogr.* **59,** 38–44
34. Emsley, P., Lohkamp, B., Scott, W. G., and Cowtan, K. (2010) *Acta Crystallogr. D Biol. Crystallogr.* **66,** 486–501
35. Adams, P. D., Afonine, P. V., Bunkóczi, G., Chen, V. B., Davis, I. W., Echols, N., Headd, J. J., Hung, L. W., Kapral, G. J., Grosse-Kunstleve, R. W., McCoy, A. J., Moriarty, N. W., Oeffner, R., Read, R. J., Richardson, D. C., Richardson, J. S., Terwilliger, T. C., and Zwart, P. H. (2010) *Acta Crystal-*

logr. D Biol. Crystallogr. **66,** 213–221
36. Krissinel, E., and Henrick, K. (2007) *J. Mol. Biol.* **372,** 774–797
37. DeLano, W. L. (2010) *The PyMOL Molecular Graphics System*, Version 1.3r1, Schrodinger, LLC
38. Smolsky, I. L., Liu, P., Niebuhr, M., Ito, K., Weiss, T. M., and Tsuruta, H. (2007) *J. Appl. Crystallogr.* **40,** S453-S458
39. Konarev, P. V., Volkov, V. V., Sokolova, A. V., Koch, M. H., and Svergun, D. I. (2003) *J. Appl. Crystallogr.* **36,** 1277–1282
40. Svergun, D. I. (1992) *J. Appl. Crystallogr.* **25,** 495–503
41. Konarev, P. V., Petoukhov, M. V., Volkov, V. V., and Svergun, D. I. (2006) *J. Appl. Crystallogr.* **39,** 277–286
42. Dutta, S., and Tan, Y. J. (2008) *Biochemistry* **47,** 10123–10131
43. Odunuga, O. O., Hornby, J. A., Bies, C., Zimmermann, R., Pugh, D. J., and Blatch, G. L. (2003) *J. Biol. Chem.* **278,** 6896–6904
44. Shaner, L., Wegele, H., Buchner, J., and Morano, K. A. (2005) *J. Biol. Chem.* **280,** 41262–41269
45. Abbas-Terki, T., Donzé, O., Briand, P. A., and Picard, D. (2001) *Mol. Cell Biol.* **21,** 7569–7575
46. Brinker, A., Scheufler, C., Von Der Mulbe, F., Fleckenstein, B., Herrmann, C., Jung, G., Moarefi, I., and Hartl, F. U. (2002) *J. Biol. Chem.* **277,** 19265–19275
47. Kajander, T., Sachs, J. N., Goldman, A., and Regan, L. (2009) *J. Biol. Chem.* **284,** 25364–25374
48. Wang, L., Liu, Y. T., Hao, R., Chen, L., Chang, Z., Wang, H. R., Wang, Z. X., and Wu, J. W. (2011) *J. Biol. Chem.* **286,** 15883–15894
49. Hicke, L., Schubert, H. L., and Hill, C. P. (2005) *Nat. Rev. Mol. Cell Biol.* **6,** 610–621
50. Svergun, D. I., Petoukhov, M. V., and Koch, M. H. (2001) *Biophys. J.* **80,** 2946–2953
51. Volkov, V. V., and Svergun, D. I. (2003) *J. Appl. Crystallogr.* **36,** 860–864
52. Petoukhov, M. V., and Svergun, D. I. (2005) *Biophys. J.* **89,** 1237–1250
53. Doniach, S. (2001) *Chem. Rev.* **101,** 1763–1778
54. Bernadó, P., Mylonas, E., Petoukhov, M. V., Blackledge, M., and Svergun, D. I. (2007) *J. Am. Chem. Soc.* **129,** 5656–5664
55. Schlegel, T., Mirus, O., von Haeseler, A., and Schleiff, E. (2007) *Mol. Biol. Evol.* **24,** 2763–2774
56. Buchanan, G., Ricciardelli, C., Harris, J. M., Prescott, J., Yu, Z. C., Jia, L., Butler, L. M., Marshall, V. R., Scher, H. I., Gerald, W. L., Coetzee, G. A., and Tilley, W. D. (2007) *Cancer Res.* **67,** 10087–10096
57. Shih, S. C., Prag, G., Francis, S. A., Sutanto, M. A., Hurley, J. H., and Hicke, L. (2003) *EMBO J.* **22,** 1273–1281
58. Kohl, C., Tessarz, P., von der Malsburg, K., Zahn, R., Bukau, B., and Mogk, A. (2011) *Biol. Chem.* **392,** 601–608
59. Rabu, C., Wipf, P., Brodsky, J. L., and High, S. (2008) *J. Biol. Chem.* **283,** 27504–27513
60. Abell, B. M., and Mullen, R. T. (2011) *Plant Cell Rep.* **30,** 137–151
61. Borgese, N., and Fasana, E. (2011) *Biochim. Biophys. Acta* **1808,** 937–946
62. Kriechbaumer, V., von Loffelholz, O., and Abell, B. M. (2011) *Protoplasma*, in press